



Low-macroscopic field emission structure: Using the shape of the conductor to identify a local difference in electric potential

L Lapena, A Degiovanni, V Tishkova, E. Salançon

► To cite this version:

L Lapena, A Degiovanni, V Tishkova, E. Salançon. Low-macroscopic field emission structure: Using the shape of the conductor to identify a local difference in electric potential. Journal of Vacuum Science and Technology, inPress. hal-03523395

HAL Id: hal-03523395

<https://amu.hal.science/hal-03523395>

Submitted on 12 Jan 2022

HAL is a multi-disciplinary open access archive for the deposit and dissemination of scientific research documents, whether they are published or not. The documents may come from teaching and research institutions in France or abroad, or from public or private research centers.

L'archive ouverte pluridisciplinaire **HAL**, est destinée au dépôt et à la diffusion de documents scientifiques de niveau recherche, publiés ou non, émanant des établissements d'enseignement et de recherche français ou étrangers, des laboratoires publics ou privés.

Low-macroscopic field emission structure:

Using the shape of the conductor to identify a local difference in electric potential

L. Lapena, A. Degiovanni, V. Tishkova, and E. Salançon¹
CINaM, Aix-Marseille Univ, CNRS, UMR7325, France

(Dated: 21 December 2021)

The emission of electrons from an insulating crystal deposited on a conductor occurs at a macroscopic electric field of a few volts per micrometer, three orders of magnitude below the field emission from a clean metal. This is due to the local field enhancement induced by the presence of the insulating crystal. The emission profiles depend on the shape of the conductive substrate; analyzing these profiles enables the local difference in electric potential and the opening angle to be traced. Given the thickness of the crystal, the local difference in potential indicates the local field enhancement of a few volts per nanometer applied to the conductor.

Field emission is usually achieved by negatively biasing a tip of conductive material against a counter electrode placed in an ultra-high vacuum chamber^{1,2}. But although metallic ultra-thin tips are the objects most commonly used to produce strong electric fields, there is another way of obtaining field emission: at an interface between an insulating crystal and a conductor³⁻¹⁰. This kind of structure appears to enhance electric fields sufficiently to produce field emission. Based on this principle, an electron source whose construction was detailed and presented in an article in the Journal of Visualized Experiments¹¹ made it possible to achieve electron field emission with brightness¹² of the order of $B = 10^{10} A.cm^{-2}.sr^{-1}$, i.e. brightness equivalent to that of ultra-thin metal tips. This electron source consists of an insulating crystal, a rectangular plate ($1\mu m \times 500nm \times 20nm$) of celadonite, deposited on the end of a conductive carbon fiber (diameter: $\phi = 10\mu m$) polarized at an applied negative potential of the order of $V = -1kV$ with respect to an extractor located a few millimeters away. Although the macroscopic field of a few volts per micrometer is too low to produce field emission, it has been suggested that the charge of the insulating particle generates sufficient local field enhancement to produce field emission¹⁰. Electronic images obtained with a projection microscope show the point-like nature of the emission: edge fringes are clearly visible¹². Before choosing the final configuration¹¹ for the projection microscope, several different conductive supports were used, and their shape was observed to influence the emission profile. This article demonstrates how the electron extraction energy and the opening angle can be deduced from these observations.

Principle of measurements - Several supports were used for the study: carbon films, the end of a carbon fiber, and the edge of a carbon fiber (see table I). The insulating crystal deposition procedure is the same for all the supports. A small quantity of powder is weighed and then dispersed by ultrasound in a predetermined volume of water. Next, a pipette, or even a micro-pipette, is used to deposit a drop of water loaded with insulating crystals on the conductive surface. The water evaporates and the insulating crystal remains attached to the surface. The density of the deposit depends on the density of the solution and the volume of the drop.

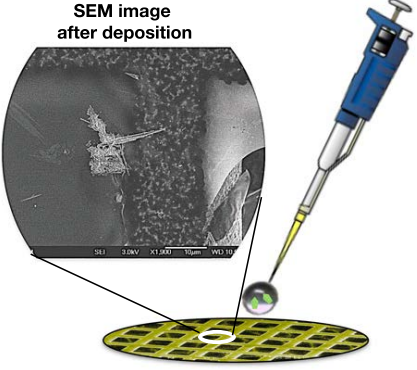
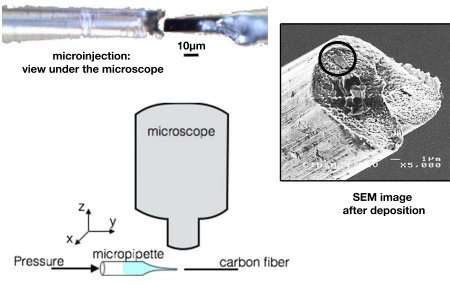
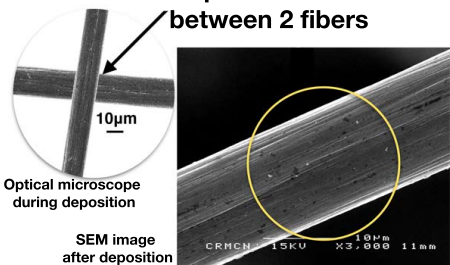
Shape of the support	Type of deposit - SEM or TEM image
Carbon film	<p>Pipette - $10\mu L$ drop deposit</p> 
End of a carbon fiber	<p>Micropipette - Capillary deposit</p> 
Edge of a carbon fiber	<p>Drop deposit between two crossed fibers</p> <p>Drop sandwiched between 2 fibers</p> 

TABLE I: Shapes of supports and methods of drop deposition

- When the support is a carbon film, it is supported on a copper grid, general practice in transmission electron microscopy. A pipette is used to place a drop of $10\mu\text{L}$ on the surface. The insulating crystals remain on the carbon film as the drop evaporates.
- Using the end of a carbon fiber as support allows the exact location of deposit, and thus of emission, to be determined. Deposition is by "capillary" deposit via a stretched pipette whose final diameter measures between 5 and $20\mu\text{m}$, controlled by a pressure system. The drop is deposited at the end of the fiber, under optical microscope.
- The carbon fiber-edge support consists of a carbon fiber of $\phi = 10\mu\text{m}$ diameter. A drop is deposited using an extra fiber perpendicular to the first; the drop is sandwiched between the two fibers. Only a few insulating crystals remain on the edge of each fiber.

To realize the emission, the source is placed under vacuum ($P \approx 10^{-5}\text{Pa}$) in front of a grid positioned between $d = 0.5\text{mm}$ and $d = 2\text{mm}$ away (see figure 1, which acts as an extractor. A fluorescent screen is positioned at $D = 6\text{cm}$ from the source. Knowing the carbon grid mesh, we deduce $d = \frac{D}{G}$ from magnification: $G = \frac{z_s}{z_f}$ (z_s corresponds to the expansion of the image on the screen, and z_f to the known size of the extractor grid).

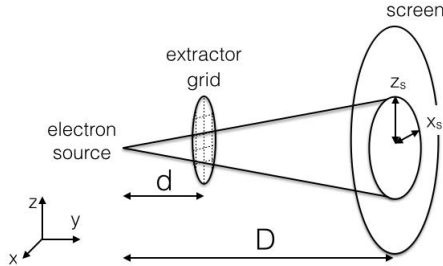


FIG. 1. Scheme of the experiment. The source-extractor distance is d and the source-screen distance is D . z_s is the vertical expansion of the image and x_s , its horizontal expansion.

The emission profiles visible on the screen shown in figure 2 are essentially determined by the geometry of the conductive substrate. When the insulating crystals are deposited on a flat surface (carbon films), the divergence of the beam produced by one crystal is about $\alpha_p = \text{atan} \frac{z_s}{D} = \text{atan} \frac{x_s}{d} = (5 \pm 2)^\circ$.

When the insulating crystal is deposited at the end of the carbon fiber, the emission profile is symmetric and the angle is always large, about $\alpha_e = \text{atan} \frac{z_s}{D} = \text{atan} \frac{x_s}{D} = (30 \pm 5)^\circ$. Finally, when the insulating crystals are deposited on the edge of the carbon fiber, the beam has an elliptical shape, with its major axis perpendicular to the fiber axis: divergence in the axis of the fiber is about $\alpha_h = \text{atan} \frac{x_s}{D} = (9 \pm 1)^\circ$ and divergence

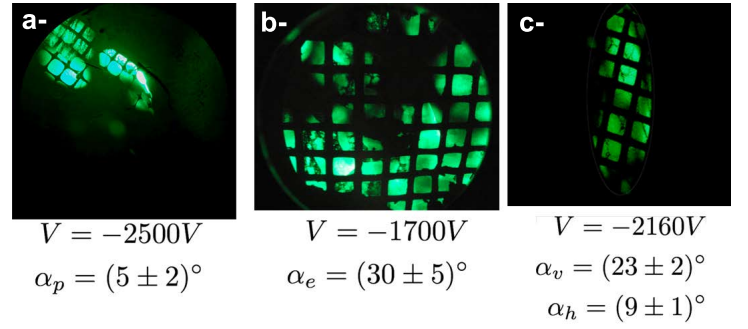


FIG. 2. Emission profiles obtained for a given type of potential applied to the deposited structure a- on a carbon film ($V = -2500\text{V}$) b- at the end of the carbon fiber ($V = -1700\text{V}$) and c- on the edge of the carbon fiber ($V = -2160\text{V}$).

in the axis perpendicular to the fiber is about $\alpha_v = \text{atan} \frac{z_s}{D} = (23 \pm 2)^\circ$. Figure 2 shows the three situations.

First analysis - Regardless of the local topography of the electric field, the source can be identified as point-like. Electrons are extracted from the conductor, at an initial velocity (\vec{v}_i) fixed by a local difference in potential ΔV_{loc} (see figure 3) before the particles are deflected by the macroscopic field (\vec{E}). The electric field topography depends on the macroscopic geometry of the electrodes. For this local difference in potential ΔV_{loc} , the initial velocity can be expressed as: $v_i = \sqrt{\frac{2e\Delta V_{loc}}{m}}$ (e corresponds to the electron charge and m to its mass).

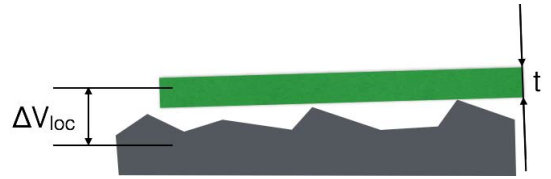


FIG. 3. The insulating crystal is charged, i.e. represented as an electric potential difference ΔV_{loc}

Under these conditions, the electrons reach a speed that creates a point-like source within the first nanometers. Their trajectory in the macroscopic field can then be analyzed according to electrode shape (see figure 4): (i) the carbon film acting as a plane electrode, the electric field is constant; (ii) the end of the carbon fiber acting as a "spherical" electrode, the electric field is radial; and (iii) the edge of the carbon fiber acting as a cylindrical electrode, the electric field is radial perpendicularly to the fiber axis.

The shape of the electron profile can be used to trace the point-like source electrons' initial velocity (v_i) and opening angle (α_i). The symmetry of the different situations helps to solve the problem of finding the kinetic energy and the opening angle of the point-like source.

In the first case, that of the carbon films, the force imposed on the emitted electron is constant along \vec{y} . The velocity along

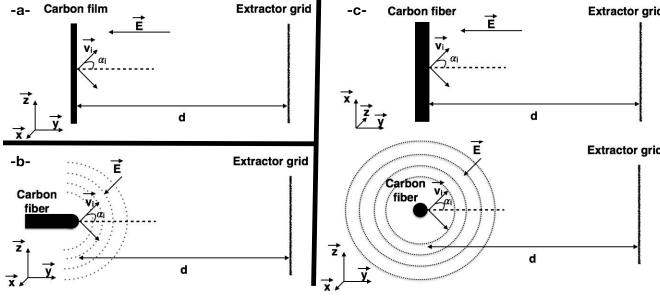


FIG. 4. Shape of the macroscopic field with the cathode negatively biased with respect to an extractor plane, when the insulating crystal is deposited on: -a- the carbon film, -b- the end of the carbon fiber, -c- the edge of the carbon fiber in two directions

\vec{x} does not change and $x = v_i \sin \alpha_i t$. Along \vec{y} , the position can be expressed as: $y(t) = \frac{eV}{2md} t^2 + v_i \cos \alpha_i t$, where e is the electron charge, m , the electron mass, V , the electric potential applied to the conductor, d , the carbon film to extractor distance, v_i the initial velocity norm, α_i , the initial angle velocity and t , the time. The last position $y_f = d$ and x_f gives the final angle $\tan \alpha_p = \frac{x_f}{d} = \frac{x_s}{D}$ (recall: $\alpha_p = 5^\circ$). Using the expression of the initial velocity, the local difference in potential can be expressed as equation 1.

$$\Delta V_{loc} = \frac{V \tan^2 \alpha_p}{4 \sin^2 \alpha_i} \times \frac{1}{1 - \frac{\tan \alpha_p}{\tan \alpha_i}} \quad (1)$$

This equation cannot be solved unless the initial angle of the velocity is known. However, in the second case, that of emission produced from the end of the carbon fiber, the electric field is radial close to the fiber. Since the field norm decreases quickly, the angle of the velocity does not substantially change at greater distances from the fiber. Thus, the angle found in this case can be considered to be the angle of the initial velocity: $\alpha_i \approx \alpha_e = 30^\circ$. Using this value, the calculation of ΔV_{loc} gives a local difference in potential $\Delta V_{loc} \approx \frac{V}{110}$.

In the third case, that of emission produced from the edge of the carbon fiber, along the direction \vec{x} , similarly to the first case, no force acts on the electrons, so the component of speed parallel to the fiber does not change $\alpha_h \approx \alpha_p$. In the plane (\vec{y}, \vec{z}) , the field is radial and the final angle can be compared to the second case with $\alpha_v \approx \alpha_e$. However, when the insulating crystal is at the edge of the carbon fiber $E(x, y, z) \propto \frac{1}{\sqrt{y^2 + z^2}}$; and, when it is at the end of the carbon fiber, $E(x, y, z) \propto \frac{1}{x^2 + y^2 + z^2}$. This explains the elliptical shape observed for the last case (cylindrical electrode) and the experimental values. This qualitative analysis does not, however, take into account certain details, like the fact that the insulating crystal is not at the center of the field sphere or cylinder. A numerical method of analysis can thus be used to refine initial velocity determination.

Numerical method - The trajectories of charged particles can be calculated using Comsol Multiphysics software and the "electrostatics" and "boundary elements" interfaces. The geometry is set in accordance with each situation and a mesh is applied. To simulate the carbon fiber, a wire of $10\mu\text{m}$ diameter is placed at one end of a $1\text{mm} \times 1\text{mm} \times 2\text{mm}$ box and polarized at the applied potential. The wire is placed either along the y axis; or lengthwise along x (see figure 5). A fine mesh is chosen for the box (between 10 and $100\mu\text{m}$) and an extremely fine mesh close to the wire (between 100nm and $10\mu\text{m}$).

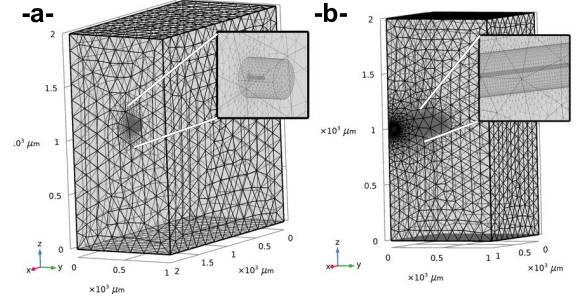


FIG. 5. Boxes and meshes chosen for the structures deposited: -a- at the end of the wire; and, -b- on the edge of the wire. The screen polarized at 0V is placed on the face of the computational box opposite the structure.

The electrostatic field is calculated numerically from Laplace's equations (see figure 6) and corresponds to that calculated analytically. When the insulating crystal is at the end of the wire simulating a carbon fiber: $E = \frac{V}{r}$, with V the potential applied to the conductor and r , its radius of curvature. When the insulating crystal is at the edge of the wire simulating a carbon fiber: $E = \frac{V}{r \ln(\frac{d}{r})}$, with V the potential applied to the conductor, d , the distance between the wire and the extractor and r the radius of the wire. In this case, a small dissymmetry appears because only the screen placed opposite the box is polarized; the other edges have no fixed potential applied.

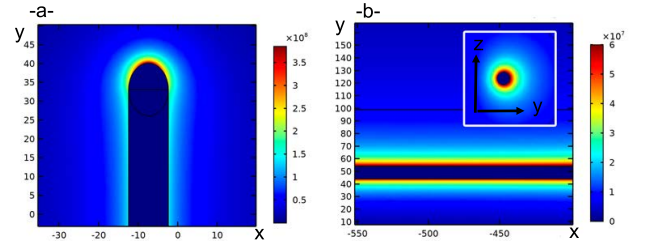


FIG. 6. Representation of the static field lines in the (x, y) plane obtained for a polarization $V = -2160\text{V}$ applied to the structures deposited a- at the end of the wire; and b- on the edge of the wire (insert: along the plane (y, z)).

Then, using the interface "particle charge tracing", the trajectories are computed dynamically with N electrons

($N = 1000$, for example) starting with an angular distribution ($2\alpha_i$) from a point, on the edge of the wire or at the end of the wire, at an initial velocity. For example, $v_i = 3.2 \times 10^6 \text{ m.s}^{-1}$ corresponds to a local difference in potential supplied to the electron of $\Delta V_{loc} = 30 \text{ eV}$.

Results and discussion - To numerically reproduce the experimental profile, adjustments can be made to the initial velocity, v_i , and to the opening angle $2\alpha_i$. In both cases, the experimentally observed emission profiles (see figure 7) are obtained.

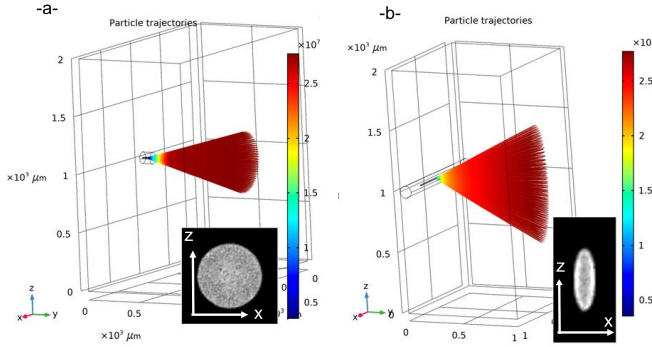


FIG. 7. Electrons acquire their velocity over the first nanometers of the structure and leave with a fixed aperture angle. The shape of the profiles is obtained for a voltage $V = -2160 \text{ V}$ applied to the structures deposited a- at the end of the wire (insert: shape obtained in the extractor plane) and b- on the edge of the wire (insert: shape obtained in the extractor plane)

But the conditions of initial velocity and cone angle applied, in particular on the edge of the wire, radically change the profile obtained. Of the set of possible conditions on these two quantities, there is one configuration of cone angle and initial speed that enables the experimental results to be reproduced (see figure 8).

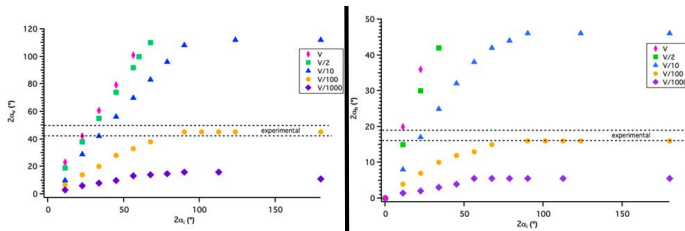


FIG. 8. Left: $2\alpha_v$, the vertical cone angle vs $2\alpha_i$, the initial cone angle; Right: $2\alpha_h$, the horizontal cone angle vs $2\alpha_i$, the initial cone angle. Results obtained for the structure deposited on the edge of the wire for different initial velocities (expressed as a proportion of the applied potential)

When emission is from the edge of the carbon fiber, profile reproduction requires the initial electron velocity to be set so as to correspond to a potential of the order of $\Delta V_{loc} \approx \frac{V}{100}$ and the initial cone angle, while less critical, must be higher than

$2\alpha_i > 60^\circ$. These values are almost identical to the results obtained in the first analysis. This means that the electron energy of the point-like source is about $e\Delta V_{loc} = 20 \text{ eV}$ when the voltage applied to the extractor is about $V = 2000 \text{ V}$, suggesting that the local difference in potential $\Delta V_{loc} = 20 \text{ V}$ is due to positive charges on the insulating crystal. From the thickness ($t \approx 20 \text{ nm}$) of the deposited crystal, we estimate the local electric field $E_{loc} = \frac{\Delta V_{loc}}{t} \approx 1 \text{ V/nm}$ applied to the carbon, which falls within the usual values for field emission: a few volts per nanometer.

Experimentally, the position and opening angle of the point-like source do not change with increasing voltage V . The intensity evolves as a Fowler-Nordeim curve $I/V^2 = f(1/V)^{11}$, indicating that the local field is increasing proportionally to the macroscopic field. This is confirmed by the model. In the case of the end of the fiber, for a potential of $V = -2160 \text{ V}$, the field is 6 times higher (red scales in figure 6) than the field on the edge of the fiber. At this potential, to reproduce the shape obtained experimentally ($2\alpha_e \approx 60^\circ$) when emission is produced from the end of the carbon fiber, $\Delta V_{loc} = 140 \text{ V}$ must be applied, in other words a local difference in potential 6 times higher than on the edge of the fiber and proportional to the macroscopic field. Note that the emission intensity is much higher in figure 2b than in figure 2c.

Finally, the accuracy of point-like source positioning in the numerical model is defined by the mesh, which is $\pm 100 \text{ nm}$. This is not a critical factor in reproducing the overall shape and only impacts the angle of the initial velocity. With this model, the position of the virtual electron source is not determined precisely enough to accurately position the point-like source.

In conclusion, the velocity and the opening angle of the point-like source electrons produced by an insulating crystal on a conductor are deduced from the electron emission profile. Depending on the topography of the geometry of the cathode where the insulating crystal is placed - a carbon film - the edge of a carbon fiber - or - the end of a carbon fiber - the divergence of the beam changes. The nature of these changes depends on how the macroscopic electric field curves the trajectories of electrons. The beam divergence angle is then used to determine the point-like source characteristics (velocity and opening angle) before they are subjected to a macroscopic field of a few $\text{V}/\mu\text{m}$. This initial velocity can be attributed to an enhancement of the local field induced by sufficient positive charges on the insulating crystal. A local difference in potential of the order of 20 V positive with respect to the conductor is deduced from analytical analysis and confirmed using a numerical method. This involves a local field of some V/nm , as expected with field emission. The shape of the conductive support influences the electron emission profile for this kind of electron source. The shape of the support could be adjusted in line with the chosen divergence angle, within a range of $10^\circ < 2\alpha < 60^\circ$. Further work is required to identify a method of determining precisely the local electric field enhancement produced by crystals. Nevertheless, we have defined the local difference in potential and the size of crystal required for the enhancement. An interesting extension would

be to compare local differences in potential according to the thickness and the nature of the crystal used.

ACKNOWLEDGMENTS

The authors would like to thank Marjorie Sweetko for improving the English of this article.

- ¹E. W. Muller and T. T. Tsong, "Field ion microscopy principles and applications," American Elsevier Pub. Co (1969).
- ²R. Gomer, "Field emission and field ionization," American Institute of Physics (1993).
- ³M. W. Geis, J. A. Gregory, and B. B. Pate, "Capacitance-voltage measurements on metal- siO₂- diamond structures fabricated with (100)- and (111)-oriented substrates," IEEE TRANSACTIONS ON ELECTRON DEVICES **38**, 619–626 (1991).
- ⁴C. Wang, A. Garcia, D. C. Ingram, M. Lake, and M. E. Kordes, "Cold field emission from cvd diamond films observed in emission electron microscopy," Electronics Letters **27**, 1459 (1991).
- ⁵K. Okano, S. Koizumi, S. Ravi, P. Silva, and G. A. J. Amaratunga, "Low-threshold cold cathodes made of nitrogen-doped chemical-vapour-deposited diamond," Nature **381**, 140 (1996).
- ⁶F. Charbonnier, "Arcing and voltage breakdown in vacuum microelectronics microwave devices using field emitter arrays: Causes, possible solutions, and recent progress," Journal of Vacuum Science and Technology B **16**, 880 (1998).
- ⁷M. Geis, J. Twichell, and T. Lyszczarz, "Diamond emitters fabrication and theory," Journal of vacuum science & technology B **14**, 2060 (1996).
- ⁸W. Zhu, G. Kochanski, and S. Jin, "Electron field emission properties of diamond," Mat. Res. Soc. Symp. Proc. **416**, 443 (1996).
- ⁹P. K. Baumann and R. J. Nemanich, "Chap. 15 : Electron emission from cvd-diamond cold cathodes," Low Pressure Synthetic diamond, Springer series in materials processing, B. Dischler & C. Wild , 281 (1998).
- ¹⁰E. Salançon, R. Daineche, O. Grauby, and R. Morin, "Single mineral particles makes an electron point source," J. Vac. Sci. Technol. B **33**, 030601 (2015).
- ¹¹E. Salançon, A. Degiovanni, L. Lapena, M. Lagaize, and R. Morin, "Preparing a celadonite electron source and estimating its brightness," Journal of visualized experiments : JoVE **153** (2019).
- ¹²E. Salançon, A. Degiovanni, L. Lapena, M. Lagaize, and R. Morin, "A low-energy electron point-source projection microscope not using a sharp metal tip performs well in long-range imaging," Ultramicroscopy **200**, 125–131 (2019).